Nanoscale Block Copolymer Templates Decorated by Nanoparticle Arrays

Ranjan D. Deshmukh,† Gavin A. Buxton,‡ Nigel Clarke,‡ and Russell J. Composto*,†

Department of Materials Science and Engineering and Laboratory for Research on the Structure of Matter, University of Pennsylvania, Philadelphia, Pennsylvania 19104-6272, and Department of Chemistry, University of Durham, Durham, UK

Received April 3, 2007; Revised Manuscript Received June 4, 2007

ABSTRACT: We present a novel one-step assembly process that encompasses in-situ formation of silver nanoparticles (NP), directed assembly of block copolymers into a perpendicular lamellar morphology, and NP organization into patterned arrays. This process utilizes organometallic precursors that thermally decompose and form spatially organized NP arrays on the free surface of the block copolymer. As NP concentration increases, the conversion of perpendicular to parallel lamellar morphology at the free surface slows down. A cell dynamical system (CDS) simulation captures the dynamics of this reorganization. The final structure is attractive for producing nanodevices because the surface is decorated by NP that are arranged in parallel arrays with tunable NP separation.

Introduction

Macromolecular self-assembly has the potential to address the ever-growing demand for arranging nanostructures that serve as building blocks for sensor, photonic, and nanobiodevices.[1−4] For example, block copolymers films and bulk samples have been used to spatially organize nanoparticles (NP).[5−14] To fully utilize their advantageous magnetic,[15] electronic,[5,16] catalytic,[17] and optical[18,19] properties, NP must be patterned and accessed over large areas with nanoscale precision and selectivity. Recently, an electrodynamic focusing method was able to direct and assemble silver NP on a prepatterned substrate with high resolution.[20] Previously, NP have been arranged on the surface of block copolymers by first assembling a block copolymer film and then depositing NP.[5,8−10,21] For example, Russell and co-workers[21] demonstrated that cadmium selenide (CdSe) nanorods surface-functionalized by a poly(ethylene oxide) (PEO) brush assembled selectively on the PMMA domains of a poly(styrene-*b*-methyl methacrylate) (PS-*b*-PMMA) film. Previously, NP have also been incorporated within the block copolymer films.[11−14,22−36] Notably, Cohen and co-workers[29−32] synthesized "organometallic block copolymers" in which an organometallic was attached to one of the blocks and then thermally decomposed to produce Pd, Au, or Ag NP within the block copolymer domain. This group also showed that dicobalt octacarbonyl, iron pentacarbonyl, and bis(cyclopentadienyl)nickel (nickelocene) complexes thermally decomposed in poly(styrene-*b*-2-vinylpyridine) (PS-*b*-P2VP) to produce metal or metal alloy NP.[33,34] Horiuchi et al.[35,36] demonstrated that metal clusters of Pd and Co could be produced in block copolymers by exposing the polymer to vapors of a precursor such as $Pd(acac)_2$ or $Co(acac)_2$, where acac is acetylacetonato. In the present paper, we demonstrate a one-step process for preparing NP during block copolymer assembly and rearrangement. Novel findings from our studies are that the unmodifed NP (i.e., no surface functionalization) segregate to the surface, slow down copolymer ordering, and partition into the PMMA domains near the surface.

In addition to their technological interest, NP incorporated into block copolymers are of fundamental interest because their size, surface functionality, and concentration influence block copolymer assembly and morphology. For example, surface-modified Au NP were found to induce a transition from lamellae to cylinders,[26] whereas cadmium sulfide (CdS) NP converted cylinders to lamellae.[28] In bulk samples, the location of NP was shown to depend on NP−domain interactions as well as NP size relative to the domain spacing.[11,12,22] For a block copolymer confined between walls, simulations[37,38] showed that NP segregated to walls and induced a transition from parallel to perpendicular lamellae at a critical loading. For PS-*b*-P2VP films, Russell and co-workers[23] showed that cylindrical P2VP domains could be oriented normal to free surface by adding tri-*n*-octylphosphine oxide (TOPO)-coated CdSe NP, which partition into P2VP and segregate to the free surface upon thermal annealing. Using grazing-incident small-angle X-ray scattering (GISAXS) to investigate this system, they showed that ordering of the cylindrical P2VP domains starts at the air surface, due to surface-segregated CdSe, and then propagates into the film.[24] Using solvent annealing, TOPO-coated CdSe NP mixed with PS-*b*-P2VP partitioned into PS domains, segregated to the free surface with >75% lateral loading, and only slightly affected the longer length scale self-assembly of diblock copolymer.[25]

The present paper describes a one-step process to prepare a nanostructured polymeric film. Individual steps include the formation of silver NP concurrent with block copolymer assembly as well as the partitioning and segregation of NP near the surface region. Prior studies in our laboratory have shown that the thermal decomposition of (1,1,1,5,5,5-hexafluoroacetylacetonato)silver(I) (AgHFA) in a poly(methyl methacrylate) (PMMA) film results in NP of Ag that segregate to the free surface.[39] Here we investigate Ag NP formation in diblock copolymer films of PS-*b*-PMMA and utilize the favorable Ag−PMMA interaction[40] to selectively partition NP in PMMA domains. During their formation, NP segregate to the surface and substrate (see Supporting Information). Concurrently, PS-*b*-PMMA chains assemble into lamellar layers that lie perpendicular to the surface (PerLam). A distinct feature of our work is that NP form "in-situ" during the assembly of the block

* To whom correspondence should be addressed: Tel 215-898-4451, Fax 215-573-2128, e-mail composto@seas.upenn.edu.
† University of Pennsylvania.
‡ University of Durham.

10.1021/ma0707943 CCC: $37.00
Published on Web 07/27/2007

copolymer and segregate to the free surface, whereas other studies either used preformed NP[23−25] or, in the case of in-situ NP,[29−34] observed a uniform distribution throughout one domain. Similar to phase-separating polymer blend films,[41] our studies show that NP can also retard the kinetics of microphase separation of block copolymer films. Whereas neat PS-*b*-PMMA films reassemble into parallel lamellae (ParLam) after 4 days, films containing NP reorganize much more slowly. Also, by increasing the NP concentration, the PerLam morphology at the surface can be stabilized and the NP can be localized into linear arrays across the surface.

Experimental Procedures

Materials and Methods. In this study PS-*b*-PMMA (M_w = 74.8 kg/mol, PDI = 1.07, Polymer Source Inc.) was dissolved in toluene to prepare an 8 wt % polymer solution. 1,1,1,5,5,5-Hexafluoroacetylacetone (HFA, Sigma Aldrich) and silver acetate (Sigma Aldrich) were added to form the organometallic complex AgHFA. To ensure silver acetate complexation, HFA was added in excess (∼10 vol %). This stoichiometry was adjusted to make 0, 2, 3.5, and 5 wt % Ag in the dried film. The solution was stirred with a magnetic stirrer for ∼5 h and then filtered (pore size, 0.25 μm) to remove any suspended impurities. To create surface hydroxyl groups, silicon substrates were treated with piranha solution (70% H_2SO_4, 30% H_2O_2) for 30 min at 80 °C. Substrates were rinsed with ultrapure water (Millipore water purification system), dried under N_2 gas, and UV-ozone treated for 10 min. The polymer solutions were spin-coated (750 rpm for 2 min) on these substrates to make ∼800 nm thick films. Films were dried in a fume hood (12 h) and then in a vacuum (24 h). Films were annealed at 185 °C in a vacuum oven for 2−94 h. One film (2 wt% Ag) was annealed for 338 h.

Characterization. Scanning force microscopy (SFM, PicoPlus Molecular Imaging, Agilent Tech.) was used for surface characterization of copolymer and NP. The tips had spring constants of 40 N/m, resonant frequencies ∼300 kHz, and diameters <10 nm. Images were taken in tapping mode with scan speeds of 0.75−1.75 Hz. Picoscan 5.3.3 (Molecular Imaging, Agilent Tech.) and SPIP (Image Metrology) software were used for image analysis. Transmission electron microscopy (TEM, JEOL 2010) at 80 kV was used to characterize the copolymer morphology and NP location within the film. To prepare TEM cross sections, films were coated with an epoxy and, after curing, immersed into liquid N_2 to delaminate the epoxy/polymer bilayer from the substrate. This bilayer was ultramicrotomed into 50−70 nm sections with a diamond knife (Richtheart Jung Ultramicrotome).

Cell Dynamical System (CDS) Simulation. The CDS method simulates the diffusive dynamics of a phase-separating diblock copolymer. The model evolves the difference in concentration between the two polymer species in response to chemical potential and concentration gradients. Furthermore, long-range interactions that result from chain connectivity are incorporated to capture the microphase separation of diblock copolymers. For further information on the CDS model we refer the interested reader to the review article by Hamley.[42] The CDS model (256 × 256 × 50) used periodic boundary conditions in *xy*-directions and no flux in the *z*-direction. The scalar order parameter $\varphi(r,t)$ describes the local concentration difference between components at position r and time t. The evolution of the order parameter is given by

$$\varphi(r,t+1) = G[\varphi(r,t)] - \langle G[\varphi(r,t)] - \varphi(r,t)\rangle - \Gamma\varphi$$

where

$$G[\varphi(r,t)] = A\tanh(\varphi(r,t)) + \frac{\partial F_{surf}}{\partial\varphi} + D(\langle\varphi(r,t)\rangle - \varphi(r,t))$$

Here, A = 1.3 and D = 0.5, corresponding to an intermediate-to-strong copolymer regime. The operator $\langle * \rangle$ represents an isotropic spatial average over neighboring modes and in three dimensions is given by

$$\langle * \rangle = \frac{6}{80}\sum_{NN} * + \frac{3}{80}\sum_{NNN} * + \frac{1}{80}\sum_{NNNN} *$$

The surface free energy accounts for the preference of one block for the substrate[43]

$$F_{surf} = \frac{\alpha}{2}\int\int \exp(-|r-s|/r_0)[\varphi(r) - \varphi_s]^2\, dr\, ds$$

where parameter α is the interaction strength at the substrate (z = 0), s is a position on the substrate, φ_s is the order parameter on the substrate, and r_0 is a length scale taken to be unity.

Results and Discussion

In this study, PS-*b*-PMMA films (ca. 800 nm) with and without AgHFA precursor were spin-coated onto silicon substrates. SFM imaging of neat, as-cast film shows random irregular features on the surface (not shown). After annealing at 185 °C for 2 h, PerLam appear as alternating stripes in the topography and phase images (Figure 1a,b). Smooth patches (arrow in Figure 1b) correspond to the ParLam with the lower surface energy PS at the air/film interface. Because of the favorable interaction, the PMMA block prefers the oxide and establishes a ParLam morphology adjacent to the substrate.[44] A mixed morphology of PerLam and ParLam at the surface has been reported.[45] In the PerLam regions, the PS striped domains are about 1 nm below the PMMA domains (Figure 1a), consistent with published studies.[46]

Annealing above the glass transition temperature of both blocks allows the ParLam regions to grow and the PerLam to shrink. Thus, after 48 h the surface mainly consists of ParLam regions (Figure 1c) that are ∼10 nm higher than the PerLam regions (inset in Figure 1c). This height difference is less than that of the bulk (L = 34 nm)[44] or thin film (40 nm) lamellae period, suggesting a nonequilibrium structure.[47] Here, we take L as 37 nm. Figure 1d reveals that the low regions in Figure 1c are PerLam whereas the high regions remain featureless, indicative of ParLam. The phase image (Figure 1e) shows that these high regions indeed correspond to the PS block, as discussed earlier. Further evidence for this assignment of morphology will be given later (Figure 3). A qualitative comparison of surface morphologies shows that the area fraction of the ParLam increases rapidly between 2 and 48 h (Figure 1b vs Figure 1e). Namely, annealing allows PS-*b*-PMMA chains within the PerLam to reorganize in order to increase the area fraction of the PS lamella parallel to the surface.

The interface between PerLam and ParLam also changes between 2 and 48 h. Initially, the PerLam stripes mainly intersect the ParLam regions at a right angle (Figure 1b), whereas after 48 h the stripes from the PerLam regions tend to align parallel to the ParLam regions (Figure 1e). Further, Figure 1e shows two ParLam regions squeezing a narrow strip of PerLam containing two or three lamella (arrow). After 96 h, the surface morphology consists of islands and holes with a height difference of 37 nm or one period (inset of Figure 1f). Although longer annealing times allow for these holes to grow,[47] the surface has already achieved a complete ParLam morphology after 96 h. The phase image (Figure 1g) shows that islands and holes have the same phase, suggesting that both regions are covered by the PS block and that the ParLam covers the entire surface.

Compared to neat PS-*b*-PMMA films, the addition of Ag NP slows down the PerLam to ParLam transition and, at high

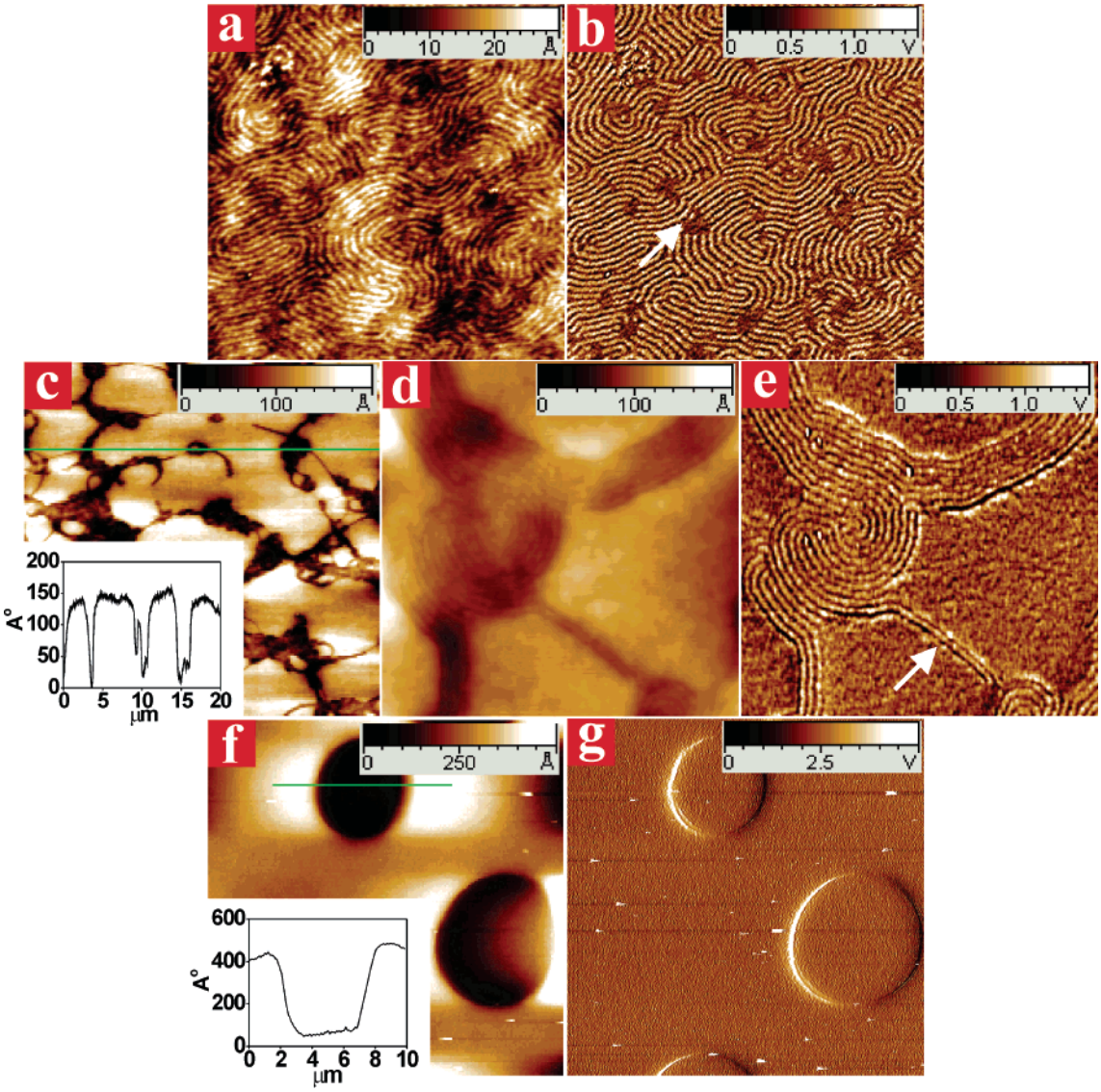

Figure 1. SFM images of PS-*b*-PMMA films showing the morphology evolution of annealed films for 2 h (a, b), 48 h (c, d, e), and 96 h (f, g) at 185 °C. Topography (a, c, d, f) and phase images (b, e, g) are shown. The insets in (c) and (f) show the height variation across the solid line in the parent image. Images are 2 μm × 2 μm (a, b, d, e) and 20 μm × 20 μm (c, f, g).

concentrations, can "freeze in" the PerLam morphology. Furthermore, NP partition into the PMMA domains and segregate to the surface. For as-cast films of PS-*b*-PMMA with AgHFA, the surface morphology is similar to that of the neat copolymer. Annealing at 185 °C decomposes AgHFA and allows the organic component to volatilize from the film. The remaining Ag^+ ions are reduced to Ag^0, which assemble into NP of Ag.[48] The interplay between NP formation and copolymer assembly during annealing can be understood by analyzing the surface and bulk morphologies characterized by SFM and TEM, respectively.

After 2 h, the surface displays a mainly PerLam morphology and Ag NP about 20 nm in diameter, as shown in Figure 2a,b. Surface segregation of Ag NP was previously observed in pure PMMA films and attributed to an incompatibility between the precursor and PMMA.[39] Rutherford backscattering spectrometry (RBS) (see Supporting Information) of PS-*b*-PMMA films containing AgHFA shows a relatively uniform concentration of Ag in as-cast films and a large surface excess upon annealing. Figure 2c shows that the Ag NP selectively assemble along the PMMA lamellae (higher stripes) on the surface. After 48 h, Figure 2d shows a mixture of ParLam (light) and PerLam (dark) regions with a height difference of 5−8 nm (inset). These regions are smaller than those in the PS-*b*-PMMA film (Figure 1c), suggesting a slower reorganization process. Similar to films annealed for 2 h (Figure 2a−c), after 48 h the NP decorate the PMMA lamellae (Figure 2e,f), suggesting a strong preference for NP to remain in PMMA even as the film transforms from a PerLam to ParLam morphology near the surface. After 96 h, the ParLam regions cover a majority of the surface, as shown in Figure 2g. The height difference between regions remains 5−8 nm (inset), which is consistent with a nonequilibrium structure (i.e., no island/hold formation). The topography and phase images (Figure 2h,i) indicate a mixture of PerLam (low with stripes) and ParLam (high and flat). After 338 h (not shown), a few islands and holes are observed, suggesting that equilibrium could be achieved after very long times. In addition to slowing the PerLam to ParLam transition, the NP disturbs the interface between the PerLam and ParLam regions. In particular, the ParLam regions are irregularly shaped throughout annealing (Figure 2f). Close inspection of Figure 2f reveals that NP tend to terminate the perpendicular PMMA domains as they impinge upong the ParLam regions. This defect structure warrants further studies. In summary, a comparison of Figures 1 and 2 shows that the addition of 2 wt % Ag NP retards

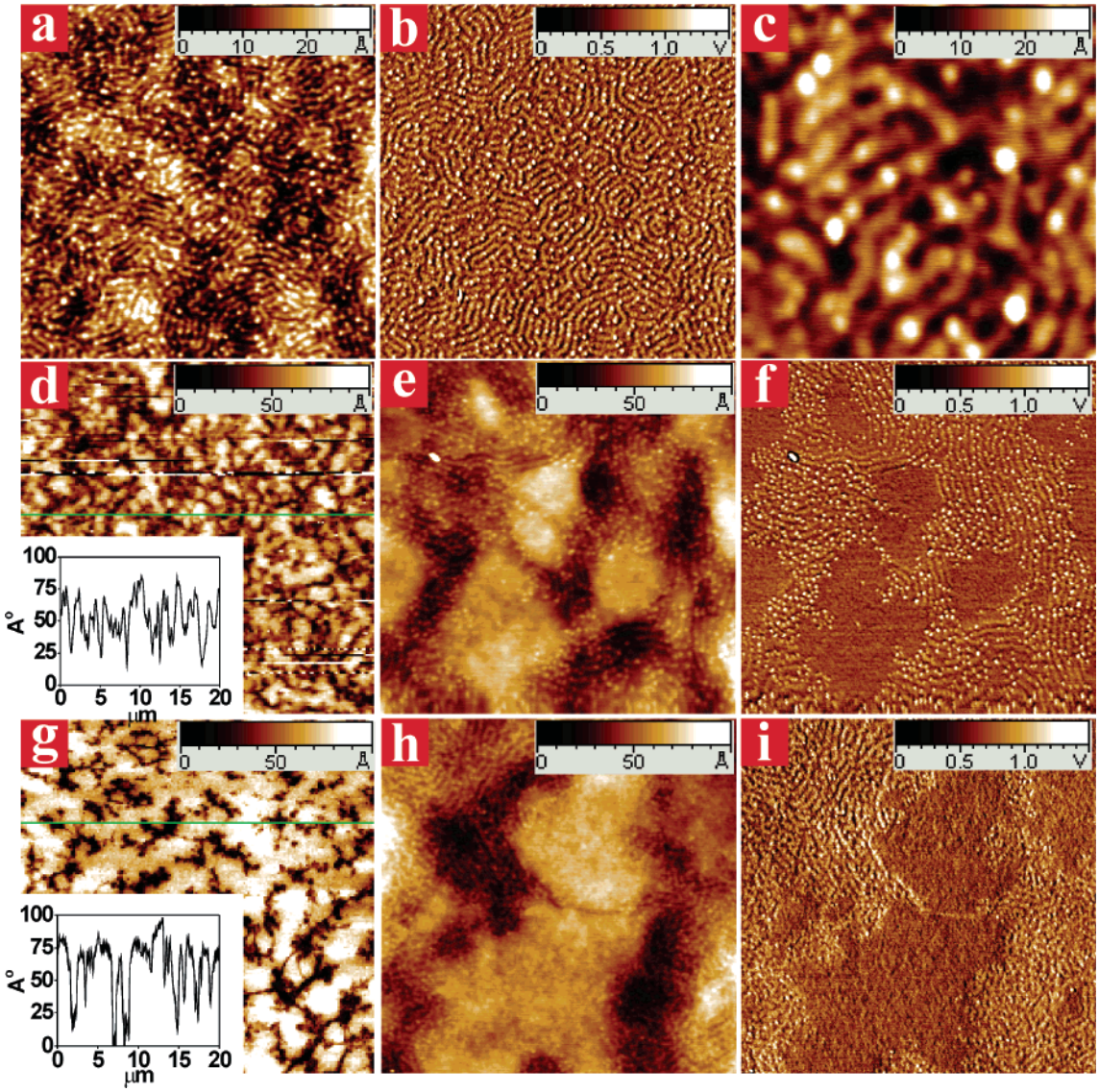

Figure 2. SFM images of PS-*b*-PMMA films with 2 wt % Ag showing morphology evolution of annealed films for 2 h (a, b, c), 48 h (d, e, f), and 96 h (g, h, i) at 185 °C. Topography (a, c, d, e, g, h) and phase images (b, f, i) are shown. The insets in parts d and g show the height variation across the solid line in the parent image. Images are 2 μm × 2 μm (a, b, e, f, h, i), 0.5 μm × 0.5 μm (c), and 20 μm × 20 μm (d, g).

the transition from PerLam to ParLam at the surface of copolymer films.

TEM images of film cross sections reveal the internal copolymer morphology as well as NP location. After 96 h, Figure 3a shows that the neat PS-*b*-PMMA film exhibits a ParLam morphology throughout the film, consistent with the island−hole structure in Figure 1f. For copolymer films with 2 wt % Ag after 48 h, NP segregate to the surface and have an average size of 17.4 ± 6.1 nm, as shown in Figure 3b. Within the bulk, smaller NP can be observed at higher magnification (Figure 3c). Note that the lamellae in Figure 3b are parallel near the substrate but mixed (ParLam and PerLam) near the surface, in agreement with the SFM images in Figure 2e,f. Arrow 1 in Figure 3b shows a transition zone where the surface PerLam merges into the ParLam below the surface. The bending of ParLam toward the surface also produces transition zones as noted by arrow 2. Note that Figure 3c suggests that NP near the surface selectively assemble inside PMMA domains (light). Because of microtoming and e-beam artifacts, TEM is used to supplement the SFM studies that demonstrate partitioning of NP in PMMA domains at the surface.

After 96 h, the diameter of NP at the surface is 17.6 ± 4.2 nm, as shown in Figure 3d,e. This size is similar to the width of individual lamella (18.5 nm), indicating that the PMMA domain size limits the growth of NP. Consistent with these measurements, NP grown in PMMA films are larger, ranging from 20 to 75 nm.[39] In PS-*b*-PMMA films, NP size remains constant with further annealing. These NP also remain near the surface, consistent with results in PMMA films. Although the ParLam morphology is prevalent in Figure 3d, regions of mixed morphology (arrow) are retained, consistent with the nonequilibrium structures in Figure 2g−i. Upon comparing Figures 3a (neat) and 3d (with NP), the addition of 2 wt % NP slows down the transition from PerLam to ParLam across the film, indicating that the NP at the surface retard the reorganization. Figure 3e shows the ParLam region after 96 h. The top PS layer (dark) contains no NP, whereas the next layer (PMMA) contains Ag NP that were originally located in the PMMA domains (stripes) of the PerLam. Smaller NP (4.1 ± 1.1 nm) are randomly dispersed below the surface and locate mainly at the PS-*b*-PMMA interface. In summary, large NP (17 nm) locate within PMMA domains at the surface, whereas small NP (4 nm)

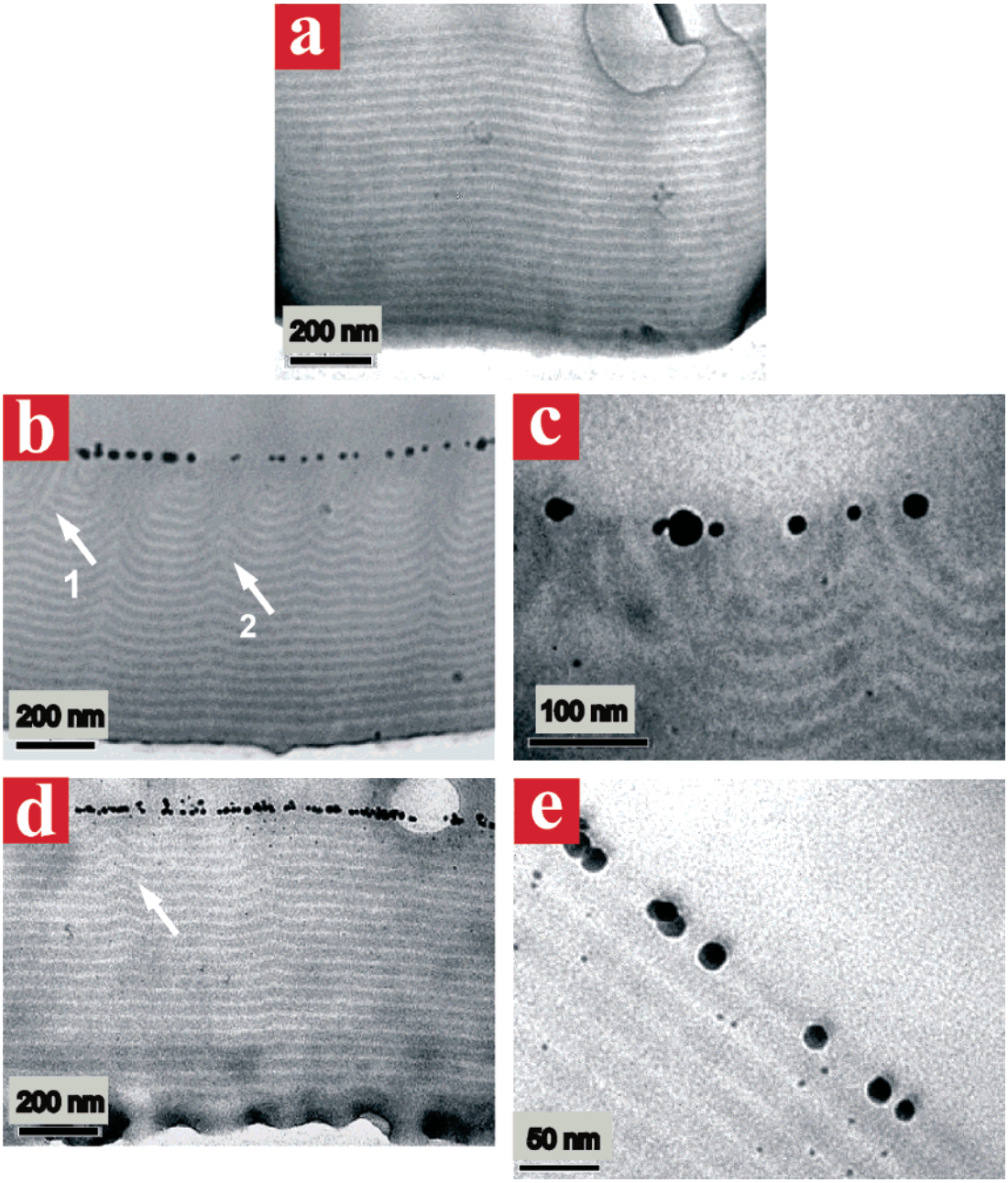

Figure 3. TEM cross sections of PS-*b*-PMMA films (800 nm) with 0 and 2 wt % Ag. (a) After 96 h, PS-*b*-PMMA films show an equilibrium morphology of ParLam; (b) after 48 h, films containing 2 wt % Ag exhibit a mixed morphology near the surface (arrow) and a ParLam adjacent to the substrate. The Ag NP partition to the surface regions. (c) is a higher magnification image of (b) taken near the surface and shows that NP terminate in PMMA domains (light stripes) of the PerLam regions. After 96 h, (d) shows that the ParLam is the majority morphology although some PerLam regions persist. (e) is a higher magnification image of (d) and shows that NP redistribute and locate in the first PMMA lamella below the surface as the PerLam morphology converts to the ParLam at the surface. Small 4 nm NP are observed below the surface in the bulk and locate at the PS/PMMA interface.

partition to the interface between PS and PMMA blocks. Mean field simulations[49,50] and experiments[22] show that small particles of diameter d satisfying $d/l < 0.2$ locate at the interface whereas large particles, $d/l > 0.3$, prefer the middle of the lamella domain, where l is the respective domain dimension ($L/2$). In this paper, the small and large Ag NP have $d/l \sim 0.2$ and 0.9, respectively, and thus their locations agree with prior studies.

The surface morphology transition in presence of NP is sketched in Figure 4. Initially (Figure 4a), the PerLam morphology dominates and NP locate along the PMMA domains (light blue) near the surface. Below the surface, the PerLam transitions to the ParLam as pointed out by Figure 3b. After annealing (Figure 4b), some regions of PerLam rearrange to form the ParLam with an outermost PS lamella that rise, $L/4 \sim 9$ nm, above the adjacent PerLam regions (cf. Figures 1 and 2). Simultaneously, NP near the surface relocate and become buried in the first PMMA layer adjacent to the surface. This behavior is supported by the smoothness of the ParLam regions (Figure 2), which are devoid of NP. Near-equilibrium conditions are represented by Figure 4c, which shows that a ParLam film that forms islands and holes because the overall thickness is not equal to $(n + {}^1/_2)L$, where n is integer. As shown in Figure 3e, the NP are now buried below the surface of the PS layer and locate in the center of the PMMA lamella.

The surface morphology of the PS-*b*-PMMA films depends on the concentration of Ag. Figures 5a,b and 5c,d correspond to 3.5 and 5 wt % Ag NP, respectively. Compared to the neat and 2 wt % Ag films, Figure 5a shows that order is greatly

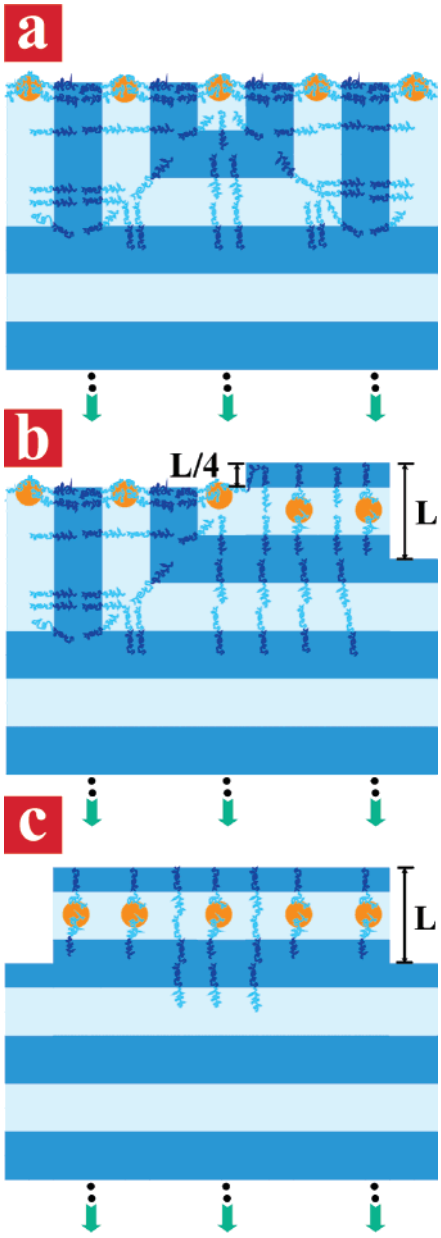

Figure 4. Near-surface region of a PS-*b*-PMMA film containing NP that shows the transition from PerLam to ParLam as well as the redistribution of NP. Color scheme: PS, PMMA, and NP are dark blue, light blue, and gold, respectively. The morphology evolution near the surface is from (a) PerLam to (b) mixed PerLam and ParLam to (c) ParLam. The NP partition into PMMA and those near the surface slow down the morphology transition. The T-junctions result from the intersection of PerLam at the free surface and ParLam from below.

reduced and the PerLam regions are small for films containing 3.5 wt % Ag after 2 h. Similar to the 2 wt % case, NP partition into the PMMA domains. After 96 h, regions of the ParLam (light) and PerLam (dark) are observed in Figure 5b. Upon increasing to 5 wt % Ag, the PerLam morphology shows only short-range order after 2 h, as shown in Figure 5c; however, after 96 h, molecular arrangements are sufficient to allow longer range order in the PerLam regions, as shown in Figure 5d. The inset of Figure 5d shows that NP on the surface not only assemble into dense arrays but also align with the PMMA domains. Because of surface segregation, the area fraction of NP is much greater than the bulk value of 5 wt %. Moreover, the conversion of PerLam at the surface to ParLam is completely suppressed at 5 wt %.

Using the SFM images, the dynamics of the surface morphology transition from PerLam to ParLam can be investigated for the neat films as well as those with NP. SFM images such as those shown in Figures 1, 2, and 5 were used to determine area fractions of PerLam by analyzing many scans taken over different areas. Figure 6 shows that the area fraction of the ParLam regions increases rapidly with annealing time for neat copolymer films, and nearly complete ParLam is achieved after 96 h (i.e., island/hole morphology). However, the transition from PerLam to ParLam slows down as the Ag concentration increases to 2 and 3.5 wt %. The addition of 5 wt % Ag to the copolymer film pins the PerLam morphology for annealing up to 96 h. Namely, the NP slow down the transition from PerLam to ParLam near the surface. As shown in Figure 3e (or 4c) the formation of the ParLam morphology would require the redistribution of surface NP to allow the copolymer molecules to rearrange near the surface (cf. Figure 4). Macroscopically, the NP increase the effective viscosity of the copolymer and thus slow down the transition from PerLam to ParLam near the surface. Recent studies of polymer blends show that NP can slow down phase separation and even stabilize bicontinuous structures at high concentrations.[41] The thickness of the films may also affect the kinetics of block copolymer/NP reorganization. For example, the surface excess of Ag in PMMA normalized by film thickness varies linearly with bulk loading of Ag. Thus, thicker films are expected to produce a higher surface density of NP, and therefore the pinning of the PerLam could occur at lower loadings than observed in this study. However, further studies are required to test the effect of thickness on the kinetics of block copolymer/NP reorganization.

In order to better understand the PerLam to ParLam transition, we use a CDS method[42,51−53] to mimic the phase separation kinetics of diblock copolymer films deposited on a selective substrate. Because it is computationally efficient, the CDS method allows one to follow morphology transitions over reasonable computational time scales. Nevertheless, dynamic computer models are unable to simulate copolymer transitions until complete equilibrium is achieved. Computer simulations of the morphology evolution are shown in a series of snapshots in Figure 7a−c where the substrate interaction strength, α, is 0.001. This value represents a relatively strong attraction of PMMA (gray) for the substrate. At early times the surface is covered with PerLam (Figure 7a), whereas the substrate induces the formation of the ParLam (not shown). At later times, however, the ParLam propagates through the film and starts to appear as islands at the surface (red patches in Figure 7b). Eventually, these islands grow and coalesce until the film consists mostly of ParLam regions (Figure 7c). Thus, the predicted appearance of ParLam islands at the surface as well as the transition from PerLam to ParLam agrees with experimental observations.

To mimic the slowing down of the PerLam to ParLam transition due to the NP, the substrate interaction parameter is reduced to weaken the driving force for ParLam to form at the substrate. Figure 7d shows the area coverage of ParLam morphology as a function of time as α is reduced from 0.001 to 0.0004. For clarity, selected images of the surface morphology are included for $\alpha = 0.001$. Decreasing α slows down the formation of the ParLam such that for systems with $\alpha < 0.0008$ the transition from PerLam to ParLam is not observed over an accessible time scale. Competing with the driving forces for phase separation, however, is the substrate interaction term, which represents the energetic preference for one component to wet the substrate. For high values of α, the "wetting"

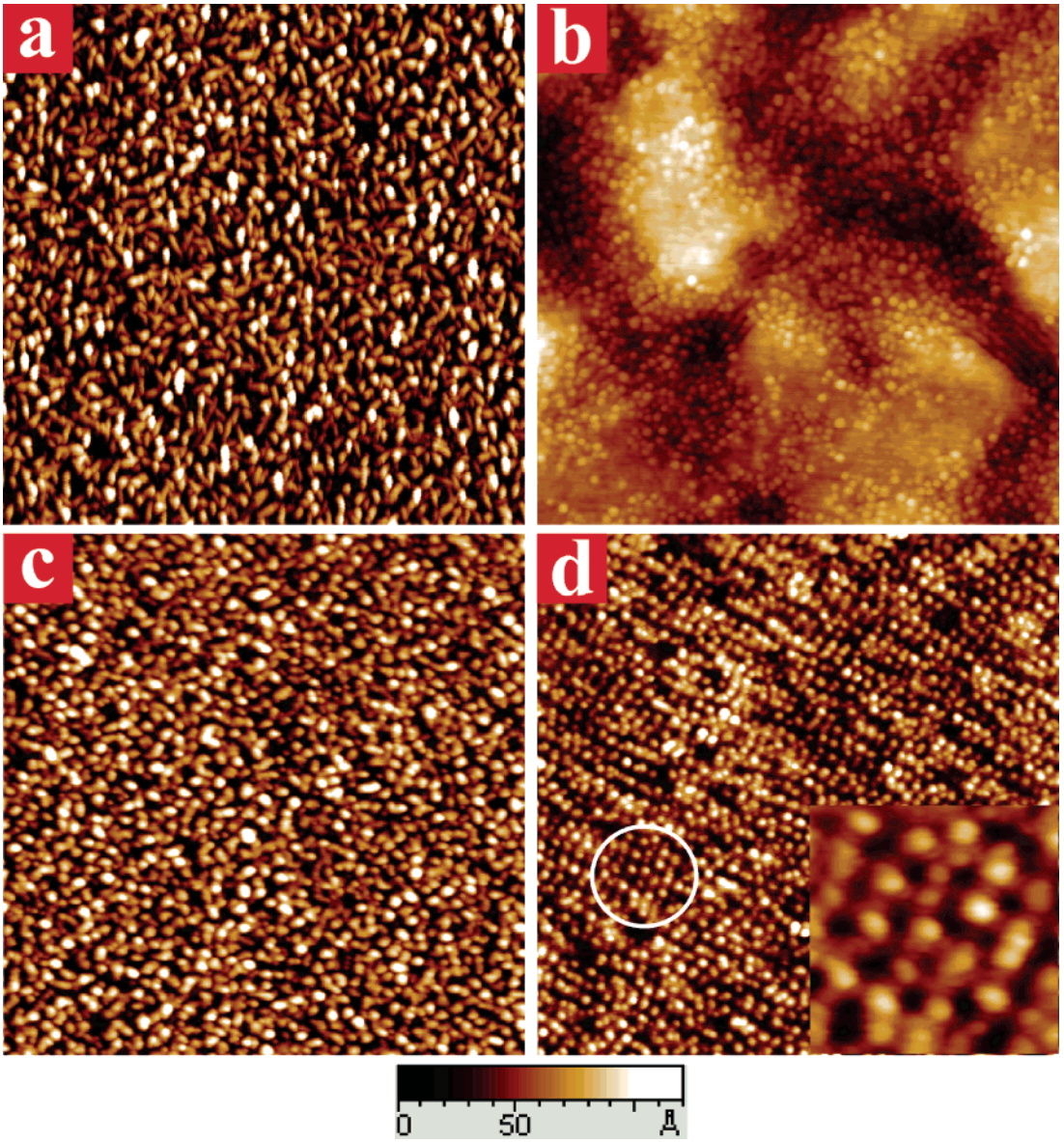

Figure 5. PS-*b*-PMMA surface morphology and NP location as a function of NP concentration. For the 3.5 wt % Ag case, topography images show the formation of (a) short-ranged PerLam after 2 h and (b) both ParLam and PerLam regions after 96 h. However, the 5 wt % Ag films show (c) irregular PerLam after 2 h and (d) a PerLam morphology with long-range order after 96 h. The inset of (d) shows that NP form a dense linear array on PMMA domains at the surface (0.25 μm $\times$ 0.25 μm). For both 3.5 and 5 wt % Ag films, the NP size at the surface (no tip deconvolution) is about 25 nm, suggesting that the PMMA domain size ($\sim$18 nm) determines the NP size. Main images are 2 μm $\times$ 2 μm.

interaction is stronger than the competing forces for phase separation and the concentration of "attractive" block is enriched at the substrate. In response to this thin layer, microphase separation occurs parallel to the film adjacent to the substrate. Upon subsequent annealing, the ParLam morphology propagates from the substrate to the top layer, resulting in well-ordered ParLam throughout the film. However, upon reducing the substrate interaction potential, the driving force for wetting the substrate with the "attractive" block is reduced, and either the polymer component takes longer to wet the substrate (and drive the transition to ParLam) or the polymer component does not wet the substrate during the simulation times considered here. In other words, reducing the substrate interaction term significantly retards both the formation of a wetting layer at the substrate and the PerLam to ParLam transition. Incorporation of NP into the block copolymer is beyond the scope of this dynamic model. However, the thermodynamics of nanoparticle dispersion has greatly progressed since the pioneering studies

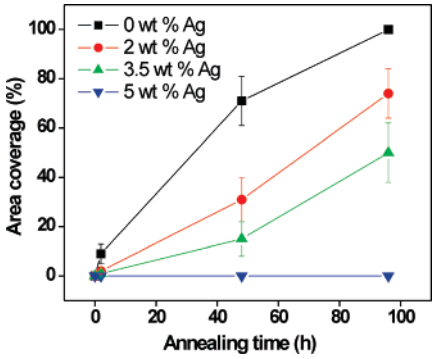

Figure 6. Area fraction of ParLam morphology vs annealing time for 0, 2, 3.5, and 5 wt % of Ag. The addition of NP slows down the PerLam to ParLam transition and at 5 wt % pins the PerLam morphology near the surface. By stabilizing the PerLam morphology, the surface provides a nanoscale pattern for organizing in-situ or preformed nanoparticles in arrays.

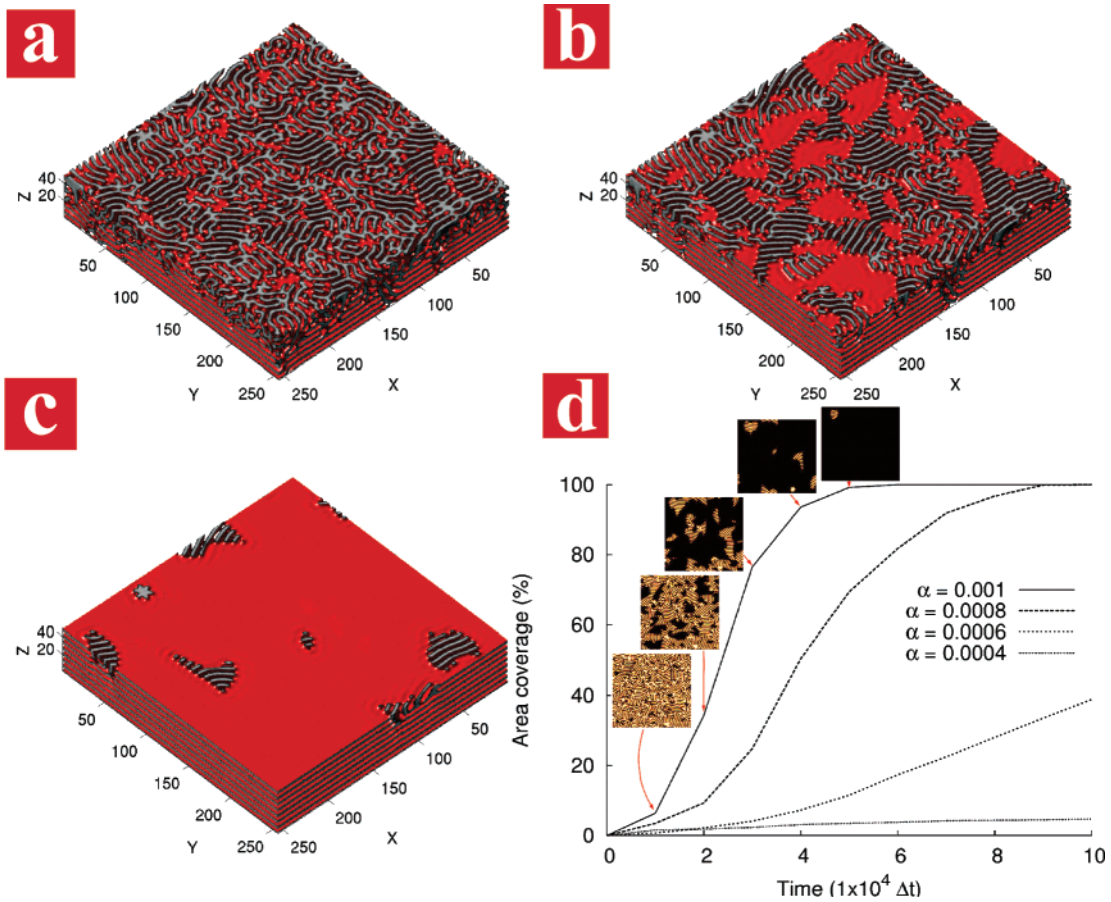

Figure 7. CDS simulations of the morphology evolution of neat copolymer films as a function of interaction strength between PMMA and the substrate, α. For α = 0.001, the surface morphology is (a) short-range PerLam at early time, (b) a mixture of PerLam and growing ParLam at intermediate time, and (c) dominated by the ParLam at late time. (d) Shows the percent area coverage of ParLam at the surface as a function of decreasing PMMA−substrate interaction. Analogous to the addition of NP, the transition from PerLam to ParLam slows down and even pins for the weakest interaction.

by Thompson, Balazs, and co-workers,[49,54] who combined self-consistent-field theory with density functional theory. In particular, Sides, Kim, Kramer, and Fredrickson[55] recently presented a powerful and flexible hybrid particle field simulation method that treats polymer and particle types that were difficult or impossible to model.

For copolymer films containing NP (cf. Figure 6), the morphological evolution is qualitatively similar to the simulations, without NP, shown in Figure 7. We emphasize that the simulations account for the slowing down of surface reorganization by decreasing the substrate potential, whereas experiments show that NP at the surface of the PMMA domains must rearrange in conjunction with the reorganization of block copolymer at the surface. Moreover, simulations of the PerLam to ParLam transition at the surface explore a shorter time scale and exhibit short-range order compared to experimental studies. Nevertheless, the simulations provide an accurate description of the surface morphology evolution in neat block copolymer films as well as a phenomenological description of the NP-containing system. Similar to the advancements in thermodynamic models,[55] new dynamic models of block copolymer nanocomposite morphology will be needed to better understand the complexity involved with NP mobility superimposed on copolymer self-assembly. In summary, the disruption of the copolymer morphology reorganization due to NP is captured in simulations by a decrease in the driving force for the ParLam to form against the substrate. Because of this decrease in preferential wetting by one block, the propagation of ParLam from the substrate toward the surface is inhibited, and thus the transformation of the surface morphology from PerLam to ParLam occurs more slowly. At high NP loading, pinning of the surface morphology is also captured by the simulations even though the mechanism differs from the experiments.

In this study, copolymer films undergo multiple processes including in-situ formation of Ag NP, surface segregation of NP, and lamellae ordering of the copolymer. Initially, PerLam lamellae appear at the surface and the only later does a PS layer form, consistent with reported neutron reflectivity experiments.[56] Thus, at short annealing times the surface acts effectively as a neutral surface that allows the PerLam to form with or without NP.[45] The strong attraction of PMMA toward silicon oxide establishes a ParLam monolayer of PS-*b*-PMMA against the substrate during solvent casting.[56] This adsorbed layer initiates the ParLam ordering front that propagates from the substrate. As captured in Figure 3b, the ParLam ordering starts from the substrate and moves toward the surface reorganizing the PerLam or randomly oriented lamellae and making them parallel. Thus, regions 1 and 2 in Figure 3b are ahead and behind the growth front, respectively. Further annealing allows the growth front to propagate toward the surface. However, before the growth front reaches the surface, the NP have segregated to the surface and reside in the PMMA domains of the PerLam morphology. The NP formation and segregation occurs faster than the block copolymer self-assembly (see RBS spectra in Supporting Information). Ag NP segregate to the surface in less than 2 h, which is much shorter time than is necessary for block

copolymer ordering (~4 days). Thus, Ag NP are located at the surface and in the PMMA domains prior to the transition of the PerLam to ParLam at the surface and affect the ordering process from the early stages. The NP provide an activation barrier for reorganizing PerLam to ParLam. Thus, the slowing down of the PerLam to ParLam at low concentrations and pinning of the PerLam at high concentrations is a result of the rapid formation and segregation of NP at the surface.

Conclusion

In this paper, in-situ formed NP are shown to modify the surface morphology of copolymer films. The addition of NP can either retard the kinetics of the PerLam to ParLam transition at the surface or pin the PerLam morphology at the surface, depending on NP concentration. The PerLam morphology, short-lived in neat block copolymers, is of great technical interest for creating alternating patterns of nanoscale dimension. Furthermore, because the NP selectively partition into the PMMA domains, parallel linear arrays of NP can be readily assembled on the surface. Such arrays may have applications for assembling new nanoscale devices.

Acknowledgment. This work was funded by National Science Foundation Polymer (DMR05-49307), MRSEC (DMR05-20020), NSEC (DMR04-25780) programs and ESPCR (GR/S96258). We gratefully acknowledge the use of the microtome in Prof. K. Winey's laboratory at the University of Pennsylvania.

Supporting Information Available: Figure S1 showing Rutherford backscattering spectra (RBS) for Ag depth profile in PS-*b*-PMMA films containing 3.5 wt % Ag. This material is available free of charge via the Internet at http://pubs.acs.org.

References and Notes

(1) Zhang, S. G. *Nat. Biotechnol.* **2003**, *21*, 1171−1178.
(2) Ikkala, O.; ten Brinke, G. *Science* **2002**, *295*, 2407−2409.
(3) Park, M.; Harrison, C.; Chaikin, P. M.; Register, R. A.; Adamson, D. H. *Science* **1997**, *276*, 1401−1404.
(4) Boal, A. K.; Ilhan, F.; DeRouchey, J. E.; Thurn-Albrecht, T.; Russell, T. P.; Rotello, V. M. *Nature (London)* **2000**, *404*, 746−748.
(5) Lopes, W. A.; Jaeger, H. M. *Nature (London)* **2001**, *414*, 735−738.
(6) Horiuchi, S.; Fujita, T.; Hayakawa, T.; Nakao, Y. *Langmuir* **2003**, *19*, 2963−2973.
(7) Aizawa, M.; Buriak, J. M. *J. Am. Chem. Soc.* **2005**, *127*, 8932−8933.
(8) Zhang, Q. L.; Xu, T.; Butterfield, D.; Misner, M. J.; Ryu, D. Y.; Emrick, T.; Russell, T. P. *Nano Lett.* **2005**, *5*, 357−361.
(9) Shenhar, R.; Jeoung, E.; Srivastava, S.; Norsten, T. B.; Rotello, V. M. *Adv. Mater.* **2005**, *17*, 2206−2210.
(10) Darling, S. B.; Yufa, N. A.; Cisse, A. L.; Bader, S. D.; Sibener, S. J. *Adv. Mater.* **2005**, *17*, 2446−2450.
(11) Chiu, J. J.; Kim, B. J.; Kramer, E. J.; Pine, D. J. *J. Am. Chem. Soc.* **2005**, *127*, 5036−5037.
(12) Kim, B. J.; Bang, J.; Hawker, C. J.; Kramer, E. J. *Macromolecules* **2006**, *39*, 4108−4114.
(13) Listak, J.; Bockstaller, M. R. *Macromolecules* **2006**, *39*, 5820−5825.
(14) Bockstaller, M. R.; Mickiewicz, R. A.; Thomas, E. L. *Adv. Mater.* **2005**, *17*, 1331−1349.
(15) Thurn-Albrecht, T.; Schotter, J.; Kastle, C. A.; Emley, N.; Shibauchi, T.; Krusin-Elbaum, L.; Guarini, K.; Black, C. T.; Tuominen, M. T.; Russell, T. P. *Science* **2000**, *290*, 2126−2129.
(16) Dietrich, C.; Koslowski, B.; Weigl, F.; Ziemann, P. *Surf. Interface Anal.* **2006**, *38*, 1034−1038.
(17) Jaramillo, T. F.; Baeck, S. H.; Cuenya, B. R.; McFarland, E. W. *J. Am. Chem. Soc.* **2003**, *125*, 7148−7149.
(18) Ishizu, K.; Furukawa, T.; Yamada, H. *Eur. Polym. J.* **2005**, *41*, 2853−2860.
(19) Wang, C. W.; Moffitt, M. G. *Langmuir* **2004**, *20*, 11784−11796.
(20) Kim, H.; et al. *Nat. Nanotechnol.* **2006**, *1*, 117−121.
(21) Zhang, Q. L.; Gupta, S.; Emrick, T.; Russell, T. P. *J. Am. Chem. Soc.* **2006**, *128*, 3898−3899.
(22) Bockstaller, M. R.; Lapetnikov, Y.; Margel, S.; Thomas, E. L. *J. Am. Chem. Soc.* **2003**, *125*, 5276−5277.
(23) Lin, Y.; Boker, A.; He, J. B.; Sill, K.; Xiang, H. Q.; Abetz, C.; Li, X. F.; Wang, J.; Emrick, T.; Long, S.; Wang, Q.; Balazs, A.; Russell, T. P. *Nature* **2005**, *434*, 55−59.
(24) He, J. B.; Tangirala, R.; Emrick, T.; Russell, T. P.; Boeker, A.; Li, X. F.; Wang, J. *Adv. Mater.* **2007**, *19*, 381−385.
(25) Zou, S.; Hong, R.; Emrick, T.; Walker, G. C. *Langmuir* **2007**, *23*, 1612−1614.
(26) Kim, B. J.; Chiu, J. J.; Yi, G. R.; Pine, D. J.; Kramer, E. J. *Adv. Mater.* **2005**, *17*, 2618−2622.
(27) Yeh, S. W.; Wu, T. L.; Wei, K. H. *Nanotechnology* **2005**, *16*, 683−687.
(28) Yeh, S. W.; Wei, K. H.; Sun, Y. S.; Jeng, U. S.; Liang, K. S. *Macromolecules* **2005**, *38*, 6559−6565.
(29) Sohn, B. H.; Cohen, R. E. *Acta Polym.* **1996**, *47*, 340−343.
(30) Chan, Y. N. C.; Schrock, R. R.; Cohen, R. E. *Chem. Mater.* **1992**, *4*, 24−27.
(31) Chan, Y. N. C.; Craig, G. S. W.; Schrock, R. R.; Cohen, R. E. *Chem. Mater.* **1992**, *4*, 885−894.
(32) Sohn, B. H.; Cohen, R. E. *J. Appl. Polym. Sci.* **1997**, *65*, 723−729.
(33) Abes, J. I.; Cohen, R. E.; Ross, C. A. *Mater. Sci. Eng., C* **2003**, *23*, 641−650.
(34) Abes, J. I.; Cohen, R. E.; Ross, C. A. *Chem. Mater.* **2003**, *15*, 1125−1131.
(35) Horiuchi, S.; Sarwar, M. I.; Nakao, Y. *Adv. Mater.* **2000**, *12*, 1507−1511.
(36) Horiuchi, S.; Fujita, T.; Hayakawa, T.; Nakao, Y. *Kobunshi Ronbunshu* **2002**, *59*, 571−577.
(37) Lee, J. Y.; Shou, Z.; Balazs, A. C. *Phys. Rev. Lett.* **2003**, *91*, 136103.
(38) Lee, J. Y.; Shou, Z. Y.; Balazs, A. C. *Macromolecules* **2003**, *36*, 7730−7739.
(39) Deshmukh, R. D.; Composto, R. J. *Chem. Mater.* **2007**, *19*, 745−754.
(40) Zeng, R.; Rong, M. Z.; Zhang, M. Q.; Liang, H. C.; Zeng, H. M. *J. Mater. Sci., Lett.* **2001**, *20*, 1473−1476.
(41) Chung, H.; Ohno, K.; Fukuda, T.; Composto, R. J. *Nano Lett.* **2005**, *5*, 1878−1882.
(42) Hamley, I. W. *Macromol. Theor. Simul.* **2000**, *9*, 363−380 and references therein.
(43) Kuksenok, O.; Jasnow, D.; Yeomans, J.; Balazs, A. C. *Phys. Rev. Lett.* **2003**, *91*, 108303.
(44) Anastasiadis, S. H.; Russell, T. P.; Satija, S. K.; Majkrzak, C. F. *J. Chem. Phys.* **1990**, *92*, 5677−5691.
(45) Sivaniah, E.; Hayashi, Y.; Matsubara, S.; Kiyono, S.; Hashimoto, T.; Kukunaga, K.; Kramer, E. J.; Mates, T. *Macromolecules* **2005**, *38*, 1837−1849.
(46) Morkved, T. L.; Lopes, W. A.; Hahm, J.; Sibener, S. J.; Jaeger, H. M. *Polymer* **1998**, *39*, 3871−3875.
(47) Collin, B.; Chatenay, D.; Coulon, G.; Ausserre, D.; Gallot, Y. *Macromolecules* **1992**, *25*, 1621−1622.
(48) Southward, R. E.; Thompson, D. W. *Chem. Mater.* **2004**, *16*, 1277−1284 and references therein.
(49) Thompson, R. B.; Ginzburg, V. V.; Matsen, M. W.; Balazs, A. C. *Science* **2001**, *292*, 2469−2472.
(50) Huh, J.; Ginzburg, V. V.; Balazs, A. C. *Macromolecules* **2000**, *33*, 8085−8096.
(51) Oono, Y.; Puri, S. *Phys. Rev. Lett.* **1987**, *58*, 836−839.
(52) Oono, Y.; Bahiana, M. *Phys. Rev. Lett.* **1988**, *61*, 1109−1111.
(53) Shinozaki, A.; Oono, Y. *Phys. Rev. E* **1993**, *48*, 2622−2654.
(54) Thompson, R. B.; Ginzburg, V. V.; Matsen, M. W.; Balazs, A. C. *Macromolecules* **2002**, *35*, 1060−1071.
(55) Sides, S. W.; Kim, B. J.; Kramer, E. J.; Fredrickson, G. H. *Phys. Rev. Lett.* **2006**, *96*, 250601.
(56) Mayes, A. M.; Russell, T. P.; Bassereau, P.; Baker, S. M.; Smith, G. S. *Macromolecules* **1994**, *27*, 749−755.

MA0707943